Reactive Growth of Nanoscale MgO Films by Mg Atom Deposition onto O_2 Multilayers

Jooho Kim,[†] Z. Dohnálek,[†] J. M. White,[‡] and Bruce D. Kay*,[†]

Pacific Northwest National Laboratory, Fundamental Sciences Directorate, Chemical Sciences Division, Richland, Washington 99352, and Center for Materials Chemistry, Texas Materials Institute, University of Texas, Austin, Texas 78712

Received: March 12, 2004; In Final Form: May 12, 2004

Nanometer thick layers of Mg metal vapor deposited onto a polycrystalline gold substrate at 22 K with and without O_2 multilayers were examined after annealing. Auger electron spectroscopy and temperature-programmed desorption of N_2 were used to determine the Mg oxidation state and the surface area of the deposits immediately after deposition at 22 K, and following annealing. Deposited on 20 layers of O_2, Mg oxidizes and forms an MgO film having a high surface area (~700 m^2/g). The surface area decreases upon annealing, approaching that of a well-ordered MgO(100) surface by 500 K. On thinner O_2 multilayers, both oxidized and metallic Mg are observed at 22 K. Mild thermal annealing (200−400 K) results in transport of the excess metallic Mg to, and alloy formation with, the underlying Au substrate. MgO films annealed to 1000 K display a narrow distribution of N_2 binding sites, similar to well-ordered MgO(100). The film sublimes above 1000 K when heated.

1. Introduction

Metal oxides are important materials in catalysis, in the environment, and in microelectronics. They are often used as supports for dispersed metal particles in heterogeneous catalysis and chemical sensor applications. The basic requirements in such applications are a high surface area (>100 m^2/g) and a high concentration of reactive sites (e.g., steps and kinks). MgO in particular has been used in a number of studies as a substrate for the deposition of metals (Ag, Fe, Ni, Pd, Cu, Pt, etc.) and as a support for finely dispersed catalytic particles.[1] MgO is also often chosen as a model ionic oxide because it has a single valence state (+2), one thermodynamically stable surface, (100), and a simple rock salt structure. Unfortunately, the large band gap (−7.7 eV) makes its characterization by electron-based surface sensitive techniques difficult because of charging. To avoid charging problems, ultrathin epitaxial films have been used in a number of studies.[2−7] Ultrathin epitaxial films of MgO(100) have been grown on a variety of substrates (Ag(100),[6−14] Mo(100),[2,3] Ru(001),[15,16] Si(100),[17] W(110),[18] GaAs(001),[19] etc.).

Both bulk and thin film MgO(100) samples have been characterized by a number of surface-sensitive techniques such as Auger electron spectroscopy (AES), ultraviolet photoelectron spectroscopy (UPS), X-ray photoelectron spectroscopy (XPS), electron energy loss spectroscopy (EELS), temperature-programmed desorption (TPD), low energy electron diffraction (LEED), and reflection high energy electron diffraction (RHEED).[2−6,8,20] Wu et al.[2,3] reported the growth of epitaxial MgO(100) thin films on Mo(100) despite a substantial lattice mismatch (−5.9%). Recently, Ag(100) has been used as a substrate for MgO(100) growth because of its small lattice mismatch of 2.9%.[6−9] Different methods of growing MgO on Ag(100) were investigated, including sputter deposition from bulk MgO,[13] oxidation of predeposited Mg layers,[6,9] and deposition of Mg in background of O_2.[6−8] The reactive deposition of Mg in an oxygen-rich environment leads to the highest quality films.[6,21,22] The surfaces of extremely thin (1−2 layers) epitaxial MgO films were also successfully imaged by STM.[23−26] At coverages of less than a monolayer, the MgO forms small islands of monatomic height, several nanometers in diameter. At higher coverage (3 ML), larger diameter (10−15 nm) domains are formed.[23−25]

Recently, our group reported a novel method, reactive ballistic deposition (RBD), for growing nanoporous MgO films.[27] These films were grown at low temperatures (≤300 K) and glancing deposition angles (≥60°). The highly porous films had large surface areas (~1000 m^2/g) and exhibited excellent thermal stability up to 1200 K. The morphology was studied by transmission and scanning electron microscopies (TEM and SEM), and the films were found to be composed of tilted arrays of nanoscale filaments with a high degree of crystallographic order and high internal surface area. The fraction of chemically active sites on these films was much larger as compared to monocrystalline MgO(100).

Over the past decade, Weaver and colleagues examined the physical vapor deposition of a wide range of materials on rare-gas multilayers.[28,29] In these studies, termed buffer-layer assisted growth (BLAG), desorption of the rare-gas buffer layer results in the formation of novel nanostructures that remain on the underlying substrate. The size distribution of the nanoclusters depends strongly on the thickness of the rare-gas multilayer. In related studies, White and co-workers recently examined the vapor deposition of Ag onto multilayer films of water adsorbed on HfO_2.[30] Subsequent desorption of the water multilayer resulted in the formation of Ag nanoclusters supported on the HfO_2 substrate.

In this study, we extend this method to include the vapor deposition of a metal, Mg, onto a potentially reactive multilayer, O_2. We demonstrate that this approach leads to the formation of nanoscale MgO films with very high surface areas. Nano-

* Corresponding author. Telephone: (509)376-0028. Fax: (509)376-6066. E-mail: bruce.kay@pnl.gov.
[†] Pacific Northwest National Laboratory.
[‡] University of Texas.

10.1021/jp040209p CCC: $27.50
Published on Web 07/02/2004

meter thick layers (≤5 ML) of Mg metal were vapor deposited onto annealed Au surfaces at 22 K covered by O_2 multilayers of varying thickness. The resulting films were characterized as a function of annealing temperature using AES, XPS, and N_2 TPD. The results show that the vapor-deposited Mg oxidizes upon deposition at 22 K, induces O_2 desorption, and forms high surface area films. If the O_2 supply is depleted, some of the deposited Mg remains metallic. Upon heating (200−400 K), the metallic Mg alloys with the underlying Au substrate.

2. Experimental Section

The experiments were performed in an ultrahigh vacuum chamber (base pressure ≈ 1.0×10^{-10} Torr) equipped with AES, XPS, LEED, and quadrupole mass spectrometry capabilities. The Mg and O_2 were deposited on an Au film prepared on Mo(100). The Mo(100) single-crystal substrate was cleaned using a standard procedure consisting of O_2 annealing at 1500 K (5 min, 1×10^{-6} Torr) followed by e-beam heating in UHV to 2000 K.[31] The temperature of the crystal was measured using a W-5% Re/W-26% Re thermocouple spot-welded to the backside of the Mo(100) sample and was varied by resistive heating from 22 to 1500 K under computer control.

Gold films were prepared by evaporating Au metal using a high-temperature effusion-cell (CreaTec) with a flux of ∼2 monolayers (ML)/min. The deposition flux was calibrated using a Quartz-Crystal microbalance (QCM XTM/2-Inficon). Gold has a number of advantages as a substrate; it is inert to oxidation, has a small lattice mismatch (3.1%) with MgO(100),[32] and can be easily desorbed from Mo(100) by annealing at ∼1500 K. After deposition, the Au films were annealed to 700 K, to increase their order. Despite the excellent homogeneity of surface binding sites as reflected in N_2 desorption (see below), the Au films did not exhibit a LEED pattern, indicating polycrystalline character. Molecular oxygen was adsorbed on the annealed Au films at 22 K. The TPD of O_2 (data not shown) displays a multilayer peak at 33 K and a monolayer desorption peak near 50 K. The absence of O_2 desorption at high temperature (∼500 K)[33−35] indicates that O_2 does not dissociate appreciably on these films.

Magnesium was dosed using an evaporator comprising a Mg ribbon (Aldrich, 99%) placed inside an Al_2O_3 tube wrapped with resistively heated tungsten wire. The source temperature was measured using a type K thermocouple cemented into the back end of the tube. The entire assembly was shielded with Ta to form a roughly collimated Mg beam. The Mg flux was measured using a QCM.

Both O_2 (NorLAB, 99.994%) and N_2 (liquid N_2 boil-off) were dosed using neat, 300 K, supersonic molecular beams directed normal to the surface. The absolute N_2 flux was calculated from the coverage-dependent sticking coefficient of N_2, the dose time leading to a saturated N_2 monolayer on MgO(100) in TPD, and the two-dimensional density of solid N_2.[36] All N_2 TPDs were measured using a line-of-sight quadrupole mass spectrometer with a linear temperature ramp rate of 0.6 K/s.

3. Results and Discussion

3.1. Surface Characterization by AES and N_2 TPD. Figure 1 shows the Mg($L_{2,3}$VV) AES spectra from the surfaces of two different Mg-containing films. Spectrum (a) was obtained after deposition of 5 ML of Mg at 22 K. The $Mg^0(L_{2,3}VV)$ AES transition is observed at 44 eV in agreement with previous studies.[2,3,37] Spectrum (b) was obtained from a 5 ML thick MgO(100) film grown by Mg deposition in a background of O_2 (∼10^{-6} Torr) at 600 K.[21] In this case, the deposited Mg is fully oxidized and only Mg^{2+} species are present.[4] The $Mg^{2+}(L_{2,3}VV)$ AES transition is observed at 32 eV and is shifted dramatically as compared to that from $Mg^0(L_{2,3}VV)$.[37] The dramatic shift (12 eV) is uncommon and is attributed to the interatomic character of the Mg^{2+} Auger process.[37] On the basis of the mean free path of 30−40 eV electrons (0.5 nm), we estimate that the Mg($L_{2,3}$VV) Auger electrons originate primarily from two topmost layers.[38]

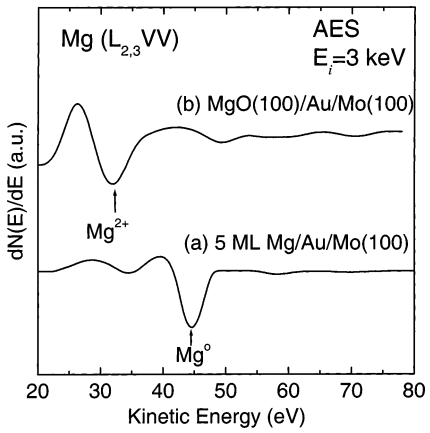

Figure 1. AES spectra of (a) 5 ML of Mg deposited on a 50 ML Au film grown on Mo(100) and (b) MgO deposited on a clean Mo(100) surface. The spectra were taken at 22 K.

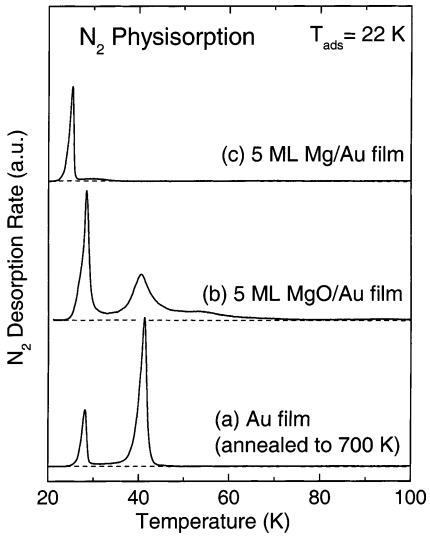

Figure 2. N_2 TPD spectra for (a) a 50 ML Au film annealed to 700 K, (b) a 5 ML MgO film, and (c) a 5 ML Mg film deposited on the annealed Au film shown in (a). The MgO film was grown in an oxygen partial pressure of 1×10^{-6} Torr. The spectra were taken using a fixed N_2 dose of 3 ML.

N_2 TPD measurements complement the Mg oxidation state results. As shown in our previous studies, N_2 TPD is an excellent tool for determining the area and distribution of binding sites on surfaces.[27,39,40] This is illustrated in Figure 2, which shows N_2 desorption spectra from (a) a 50 ML thick annealed Au film, (b) a 5 ML thick MgO film grown on the Au film, and (c) a 5 ML thick Mg film deposited on the Au film. In all cases, the substrate temperature was 22 K and the N_2 beam fluence (time-integrated flux) was 2.3×10^{15} N_2/cm^2.

The N_2 TPD spectrum in Figure 2a was obtained from a 50 ML thick, annealed Au film. It exhibits two sharp desorption features at 28 and 41 K. With increasing exposure to N_2 (data not shown), the higher temperature desorption peak appears first and saturates with the appearance of the lower temperature desorption peak. The high-temperature peak is attributed to the

N_2 that is in direct contact with the Au substrate. The low-temperature peak is ascribed to N_2 adsorbed in a second layer that is out of contact with Au. For coverages exceeding two layers, an additional unsaturable peak appears at 26 K due to the formation of N_2 multilayers. The large separation in desorption temperature between the first and second N_2 layer ($\Delta T = 13$ K) is due to a stronger van der Waals interaction between Au and the first N_2 layer than between first and second layer N_2 species. The sharpness of the N_2 monolayer TPD desorption peak demonstrates that the Au surface presents a very uniform physisorption potential to N_2, that is, a uniform distribution of binding sites for N_2. No clear LEED pattern was observed on this surface, suggesting that the Au film is polycrystalline. The annealed Au surfaces prepared in this manner were used as substrates in the Mg deposition studies discussed below. Annealing the Au is critical; without annealing, N_2 monolayer desorption is broad (40−70 K), indicating a wide, nonuniform distribution of surface binding sites. Upon annealing above 700 K, dewetting of the Au film from the Mo(100) substrate occurs.

As a reference case, we examined N_2 desorption (Figure 2b) from a 5 ML thick MgO film grown on Au by evaporation of the Mg in a background of O_2 ($\sim 10^{-6}$ Torr) at 600 K. The TPD spectrum from the first N_2 layer is composed of a peak at 41 K with a high temperature shoulder extending from 50 to 80 K. Desorption from the second layer is observed at 28 K as in Figure 2a. The TPD line shape in the monolayer desorption region is comparable to that from monocrystalline MgO(100) films grown epitaxially on Mo(100).[27] We conclude that MgO grown on annealed Au is composed predominantly of (100) terrace sites. The high-temperature desorption shoulder (50−80 K) is most likely due to morphological defects (e.g., steps and kinks).[27,40]

Figure 2c shows the N_2 TPD from a 5 ML thick, metallic Mg film deposited on annealed Au. A single unsaturable multilayer desorption feature is observed at 26 K. The absence of a distinct N_2 monolayer feature in TPD indicates that N_2 does not wet the metallic Mg surface and grows via a three-dimensional (3D) Volmer-Webber mechanism.[41] The weak interaction between N_2 and Mg leads to a small condensation coefficient at 22 K; the N_2 coverage after exposure to 2.3×10^{15} N_2/cm^2 is only 30% of that on the Au or MgO surfaces (Figure 2a and b). Importantly, the absence of an N_2 monolayer TPD peak on metallic Mg provides a convenient way of determining whether the surface of the film created by Mg deposition on O_2 multilayers is metallic or oxidized.

At first glance, it seems surprising that N_2 does not wet the highly reactive Mg surface while it readily wets the unreactive gold surface. This can be understood by considering the physisorption interaction. In physisorption, it is well known that the rare gases interact relatively strongly with transition metals and even stronger with graphite while their interaction with the alkali metals is extremely weak.[42,43] The explanation for this "chemically surprising" result is that the conduction electrons for the highly reactive alkali metals extend far out away from the surface, thereby reducing the van der Waals attraction which is the dominant interaction in physisorption. Heuristically, we expect Mg to exhibit physisorption behavior similar to that of the alkali metals because of its relatively low work function.[42,43]

3.2. Mg Deposition onto O_2 Multilayers. In this section, we describe the growth of MgO films by the deposition of Mg atoms onto O_2 multilayers on the Au film at 22 K. Monitoring the 32 AMU signal while dosing Mg indicates induced O_2 desorption (Figure 3). This is ascribed to heat released by the exothermic reaction of Mg with O_2 to form MgO (ΔH_f(MgO) $= -601.6$ kJ/mol). As the initial amount of O_2 increases, the duration of observed O_2(g) evolution also increases. Generally, for initial O_2 coverages smaller than 20 ML, the O_2 desorption signal decays before the Mg dose is completed. Based on the heat of formation of MgO and the sublimation enthalpies of O_2 (($\Delta H_{sub}(O_2) = 7.3$ kJ/mol) and Mg((ΔH_{sub}(Mg) $= 147.1$ kJ/mol),[36] the energy released is sufficient to eject 100 O_2 molecules per MgO formed. The observed O_2 desorption yield is much lower ($\sim$1 O_2 molecule per Mg), indicating that most (>99%) of the reaction exothermicity is dissipated within the film and the underlying substrate. The oscillations observed in the O_2 desorption rate arise from variations in the Mg atomic beam flux due to oscillations of ± 2 K in the temperature of the Mg evaporation source. Because of induced O_2 desorption, 20 ML or more of O_2 is required to ensure complete oxidation of 5 ML of deposited Mg. Deposition of 5 ML of Mg onto thinner O_2 multilayers results in a film comprised of a mixture of oxidized and metallic Mg (see below).

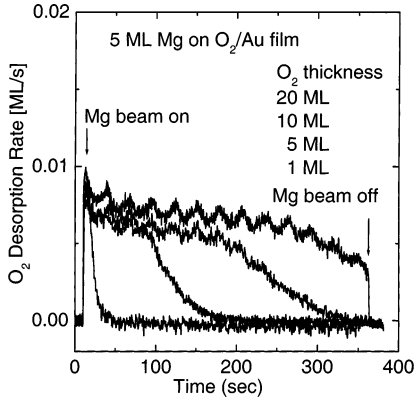

Figure 3. O_2 desorption monitored during Mg depositing onto an O_2 ice film. Oscillations in O_2 desorption rate are due to flux variations ($\pm$10%) in the Mg beam.

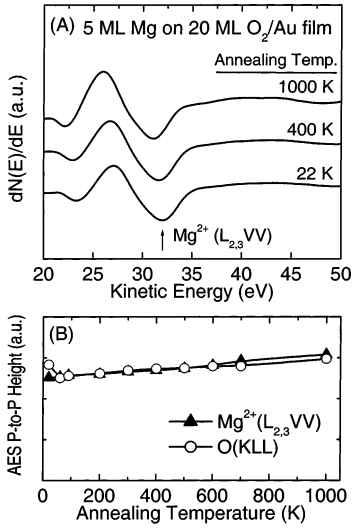

Figure 4. (A) AES spectra of 5 ML of Mg dosed onto a 20 ML thick O_2 ice. The spectra were taken at 22 K after annealing to 22, 200, 400, 700, and 1000 K. (B) Peak-to-peak height of Mg($L_{2,3}$VV) and O(KLL) AES transitions as a function of annealing temperature. Spectra demonstrate that MgO is formed at 22 K.

3.2.1. Complete Oxidation: Deposition onto Thick O_2 Layers. After deposition of 5 ML of Mg onto 20 ML of O_2 at 22 K, the Mg is fully oxidized (Figure 4A); the Mg($L_{2,3}$VV) AES transition is at 32 eV. Subsequent annealing of the film to temperatures up to 1000 K (spectra in 4A) did not lead to any

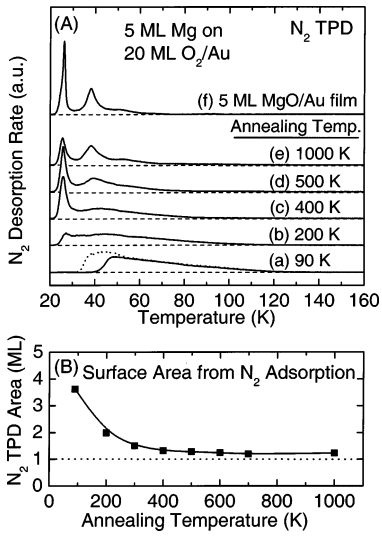

Figure 5. (A) N_2 TPD spectra from films grown by depositing 5 ML of Mg onto a 20 ML thick O_2 ice at 22 K for various annealing temperatures (a−e). N_2 TPD (f) from 5 ML of MgO on Au is shown for comparison. The dashed trace in (a) corresponds to a saturation N_2 dose at 32 K. (B) Surface area deduced from N_2 TPD as a function of annealing temperature.

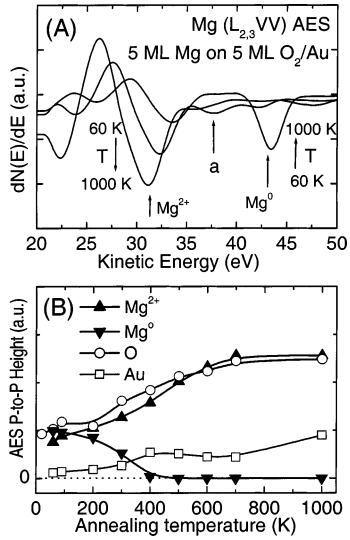

Figure 6. (A) AES spectra of 5 ML of Mg dosed onto a 5 ML thick O_2 ice. The spectra were taken at 22 K after annealing to 60, 200, 300, 400, 500, 600, and 700 K. Peak "a" corresponds to a Mg−Au alloy as discussed in the text. (B) Peak-to-peak heights of Mg($L_{2,3}$VV) (Mg^0 and Mg^{2+}), Au(N_7VV), and O(KLL) transitions as a function of annealing temperature.

significant changes in the AES peak position or line shape. There is no evidence here, or in separate XPS data (not shown), for the dewetting of Au that is observed above 700 K in the absence of the overlayer MgO film. Apparently, the MgO covering impedes restructuring of the underlying Au. The peak-to-peak intensities of the Mg($L_{2,3}$VV) and O(KLL) AES transitions both rise slowly with annealing temperature (Figure 4). The ratio is consistent and accords with that measured for epitaxial MgO(100) films. We conclude that near-stoichiometric MgO forms upon deposition at 22 K and no other compounds such as MgO_2 or Mg_2O are formed in appreciable amounts. The same conclusion has been drawn for MgO growth at 340 K where only Mg^{2+} species were observed in the films.[2,3]

Figure 5A displays N_2 TPD spectra for MgO films grown by depositing 5 ML of Mg onto a 20 ML thick O_2 multilayer at 22 K and subsequently annealing to the indicated temperatures. This TPD data parallel the AES results presented in Figure 4. For comparison, the N_2 TPD spectrum from MgO formed by Mg deposition in an O_2 background pressure at 600 K is also shown (trace f). The first N_2 spectrum obtained after Mg deposition into O_2 with subsequent annealing to 90 K (to remove excess O_2) is shown in Figure 5A(a). The onset of N_2 desorption occurs at 40 K and extends to 120 K, indicating a broad distribution of N_2 binding sites. There is no desorption from second layer N_2 at 28 K, and the total amount desorbed is 2.6 times that from a flat MgO surface. We conclude that this film has a high surface area. To determine the specific surface area of this MgO film, an additional N_2 TPD was taken (dashed line, trace a) by dosing the N_2 at 32 K instead of 22 K. At this temperature, only the first N_2 layer can be saturated, and the second and higher N_2 layers do not form at our deposition flux. The amount of N_2 adsorbed in the first layer of this MgO film is 3.7 times that of flat MgO (Figure 5A(f)). Using the known amount of deposited Mg (5 ML) and the relative area of this film with respect to flat MgO, we can estimate the specific area of the MgO in Figure 5A(a) to be 700 m^2/g.[27]

After annealing to 200 K and dosing N_2 at 22 K (Figure 5A(b)), the second N_2 layer begins to appear, indicating partial densification of the high-surface area MgO film. Annealing to 400 K (Figure 5A(c)) results in further densification, but desorption from the first layer still extends over a broad temperature range (30−90 K), indicating a broad range of adsorption sites. Annealing to higher temperatures results in a sharpening of the monolayer TPD feature, with the spectrum approaching that of a flat MgO surface (trace f) by 1000 K. Figure 5B shows the area of the N_2 monolayer TPD feature ($T > 32$ K) as a function of annealing temperature; the film exhibits nearly complete densification by 400 K. The film annealed to 1000 K retains a surface area slightly higher (∼10%) than that of the flat MgO surface (Figure 5A(f)), indicating some residual roughness.

Collectively, the TPD and AES results indicate that Mg evaporated into an excess of O_2 is fully oxidized upon deposition at 22 K, resulting in the formation of a high-surface area MgO film. This film densifies between 90 and 400 K. Further annealing to 1000 K results in a narrowing of the distribution of N_2 binding sites, ultimately approaching that of high-quality MgO(100).[27]

3.2.2. Incomplete Oxidation: Deposition onto Thin O_2 Layers. In this section, we present data obtained after the deposition of 5 ML of Mg onto a 5 ML thick O_2 multilayer, a situation where not all Mg is oxidized. The AES from a film annealed to 60 K contains both oxidized Mg^{2+} and metallic Mg^0 features (Figure 6A). The presence of metallic Mg (44 eV) confirms that the initial film contained an insufficient amount of O_2 to fully oxidize all of the Mg during the deposition.

Peak-to-peak intensities of various AES transitions, including Au(N_7VV), as a function of annealing temperature are shown in Figure 6B. The Mg^0($L_{2,3}$VV) Auger peak at 44 eV decreases and vanishes above 400 K. Conversely, the Mg^{2+}($L_{2,3}$VV) peak intensity increases with increasing annealing temperature. Because there is no unreacted oxygen and because Mg desorption (not shown) occurs at 490 K, as on Mo(100)[2,3] and Ru(100),[15] alternatives are sought to explain these results (see below). Figure 7 shows N_2 TPD spectra for the film of Figure 6. The spectra observed after annealing to temperatures lower than 200 K are dominated by a single N_2 desorption peak at 26 K characteristic of multilayer N_2. The absence of any monolayer feature in the N_2 TPD spectra indicates these films are nonwetting with respect to N_2. Further annealing in steps results

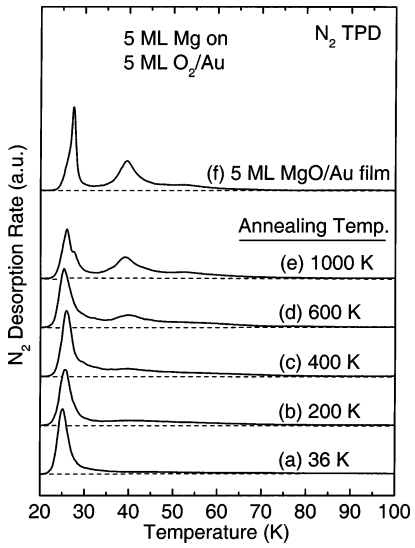

Figure 7. N_2 TPD spectra from films grown by depositing 5 ML of Mg onto a 5 ML thick O_2 ice at 22 K for various annealing temperatures (a−e). N_2 TPD (f) from 5 ML of MgO on Au is shown for comparison.

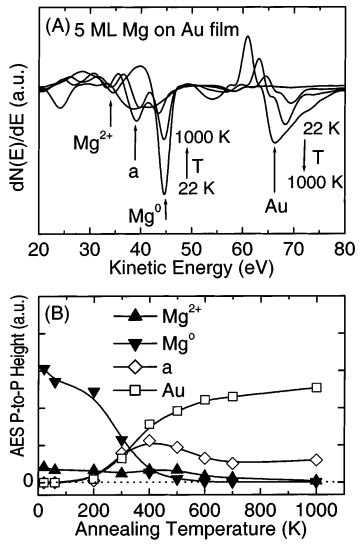

Figure 8. (A) AES spectra of 5 ML of Mg dosed at 22 K onto a Au film. The spectra were taken at 22 K after annealing to 22, 200, 300, 400, 500, 600, and 1000 K. Peak "a" corresponds to a Mg−Au alloy as discussed in the text. (B) Peak-to-peak heights of Mg($L_{2,3}$VV) (Mg^0, Mg^{2+}, and "a") and Au(N_7VV) as a function of annealing temperature.

in the appearance of a new peak at 40 K, which grows with increasing annealing temperature. By 1000 K, this peak closely resembles the monolayer desorption feature of N_2 from a well-ordered MgO film (Figure 7f).

Collectively, the combined AES (Figure 6) and TPD (Figure 7) results indicate that below 200 K the surface of the film is dominated by metallic Mg but the underlying region contains MgO even at 22 K. Heating to higher temperatures results in transport of metallic Mg to the Au substrate and the concomitant appearance of MgO at the vacuum-exposed surface. This transport occurs in the absence of Mg desorption and results in the formation of a Mg−Au alloy. Formation of a Mg−Au alloy is supported by the appearance of a new Mg($L_{2,3}$VV) AES peak at 39 eV (peak labeled "a" in Figure 6A). We believe that the transport of Mg to the Au substrate is dominated by the surface diffusion of metallic Mg on MgO to bare regions of the underlying Au substrate rather than by bulk diffusion of Mg through MgO. This is supported by experiments (not shown) that indicate Mg deposited on dense well-ordered MgO films desorbs prior to the onset of measurable diffusion into the film.

3.3. Mg Deposition onto Au: Evidence for Alloy Formation. To further confirm the alloying of Mg with the Au film, we deposited Mg directly onto a bare Au film. The AES spectra from 5 ML of Mg deposited at 22 K on a 50 ML Au film are shown in Figure 8A as a function of annealing temperature (22−1000 K). The corresponding peak-to-peak intensities of the Mg($L_{2,3}$VV) and Au(NVV) transitions are plotted in Figure 8B. The intensity of the Mg^0($L_{2,3}$VV) transition at 44 eV decreases with increasing annealing temperature and almost completely disappears by 500 K. These changes are similar to the annealing temperature dependence of Mg^0($L_{2,3}$VV) observed in Figure 6B. A small peak corresponding to Mg^{2+}($L_{2,3}$VV) is also observed. This peak is independent of annealing temperature and most likely arises from oxidation of a small fraction of the metallic Mg by background gases (H_2O, CO) during deposition. An AES peak, labeled "a", appears at 39 eV, and, as discussed above (see Figure 6), it is assigned to formation of a Mg−Au alloy. The "a" peak intensity increases with annealing to 400 K, decreases between 400 and 700 K, and then becomes constant to 1000 K.

The absence of Mg multilayer desorption indicates that Mg−Au alloy formation occurs below 490 K. A number of

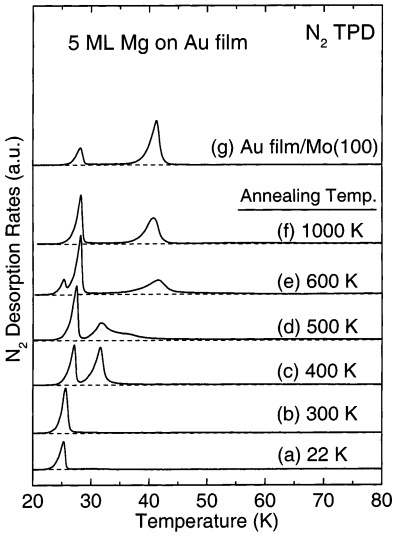

Figure 9. N_2 TPD spectra from films grown by depositing 5 ML of Mg onto a Au film at 22 K for various annealing temperatures (a−f). N_2 TPD (g) from annealed Au film is shown for comparison.

stoichiometric (Mg_3Au and Mg_2Au) and nonstoichiometric Mg−Au alloys are reported in the literature.[44] Most of these alloy phases are thermodynamically stable to very high temperatures (1000 K) and are likely to form under our experimental conditions. The alloying hypothesis is also consistent with the AES data presented in Figure 8. Below 400 K, a Mg-rich alloy forms in the near surface region (maximum in the intensity of peak "a"). Upon further annealing to 700 K, the intensity of "a" decreases due to facile diffusion of Mg into the bulk of the alloyed film. Further heating above 700 K does not yield any additional changes in the alloy peak ("a") AES intensity, indicating that Mg is distributed uniformly throughout the film.

Figure 9 displays N_2 TPD spectra corresponding to Figure 8. Up to 300 K, there is a single peak corresponding to N_2 multilayer desorption, indicating the surface is covered by metallic Mg (see discussion of Figure 2c). This agrees with the observation of pure, metallic Mg in the corresponding AES spectra (Figure 8). After annealing to 400 K, a new desorption peak appears at 32 K, indicating changes in the surface composition.

The sharpness of this peak suggests that the surface has a narrow distribution of binding sites. The precise nature of this surface is unknown, but likely has a composition of one of the stoichiometric alloys. Further annealing to 500 K leads to the appearance of a high-temperature shoulder on the 32 K TPD peak. Annealing to temperatures of 600 K and higher results in a shift of the N_2 monolayer desorption peak to 41 K. Initially, this peak is broad, but sharpens with increasing annealing temperature. At 1000 K, the peak shape approaches that observed from a clean, annealed Au substrate (Figure 9g). This is consistent with the decreased Mg concentration observed via AES (Figure 8B). The composition of Mg−Au alloy uniformly distributed throughout the film would be 10% atom Mg.

4. Summary and Conclusions

Ordered, polycrystalline Au films were prepared on a Mo(100) surface and used as substrates in a study of Mg vapor deposition and oxidation by O_2 multilayers. The composition, surface area, and distribution of binding sites of the Mg deposits were examined using N_2 uptake at 22 K and TPD as a function of annealing temperature. In the presence of excess O_2, Mg oxidizes upon deposition at 22 K, producing a high-surface area MgO film. The specific surface area of a 5 ML thick MgO film was 700 m^2/g. The film surface area decreases upon post-growth thermal annealing, approaching that of a well-ordered MgO(100) surface by 400 K. Further annealing to 1000 K leads to an MgO film with a narrow distribution of N_2 surface binding sites resembling those on single-crystal MgO(100).[27] The chemical composition of the film is independent of thermal annealing up to 1000 K, indicating that stoichiometric MgO was formed during the low-temperature oxidation. Heating above 1000 K results in sublimation of the film.

Deposition of Mg onto O_2 multilayers at 22 K that are insufficiently thick to ensure complete MgO formation results in a film containing both oxidized (MgO) and metallic Mg. In these films, the metallic Mg resides preferentially at the vacuum exposed surface. Subequent mild annealing (200−400 K) results in the transport of metallic Mg to the underlying Au substrate, accompanied by Mg−Au alloy formation.

Acknowledgment. This work was supported by the U.S. Department of Energy Office of Basic Energy Sciences, Chemical Sciences Division, and it was performed at the W. R. Wiley Environmental Molecular Science Laboratory, a national scientific user facility sponsored by the Department of Energy's Office of Biological and Environmental Research and located at the Pacific Northwest National Laboratory. Pacific Northwest National Laboratory is operated for the U.S. Department of Energy by Battelle under Contract No. DE-AC06-76RLO 1830. J.M.W. gratefully acknowledges the support as a visiting faculty member by the W. R. Wiley Environmental Molecular Science Laboratory, and by the Chemical Sciences, Geosciences and Biosciences Division, Office of Basic Energy Sciences.

References and Notes

(1) Henry, C. R. *Surf. Sci. Rep*. **1998**, *31*, 235.
(2) Wu, M.-C.; Corneille, J. S.; Estrada, C. A.; He, J.-W.; Goodman, D. W. *Chem. Phys. Lett.* **1991**, *182*, 472.
(3) Wu, M.-C.; Corneille, J. S.; He, J.-W.; Estrada, C. A.; Goodman, D. W. *J. Vac. Sci. Technol., A* **1992**, *10*, 1467.
(4) Corneille, J. S.; He, J.-W.; Goodman, D. W. *Surf. Sci.* **1994**, *306*, 269.
(5) Schaffner, M.-H.; Patthey, F.; Schneider, W.-D. *Surf. Sci.* **1998**, *417*, 159.
(6) Wollschläger, J.; Viernow, J.; Tegenkamp, C.; Erdös, D.; Schröder, K.-M.; Pfnür, H. *Appl. Surf. Sci.* **1999**, *142*, 129.
(7) Altieri, S.; Tjeng, L. H.; Sawatzky, G. A. *Phys. Rev. B* **2000**, *61*, 16948.
(8) Wollschläger, J.; Erdös, D.; Schröder, K.-M. *Surf. Sci.* **1998**, *402*−*404*, 272.
(9) Peterka, D.; Tegenkamp, C.; Schröder, K.-M.; Ernst, W.; Pfnür, H. *Surf. Sci.* **1999**, *431*, 146.
(10) Tegenkamp, C.; Michailov, M.; Wollschläger, J.; Pfnür, H. *Appl. Surf. Sci.* **1999**, *151*, 40.
(11) Altieri, S.; Tjeng, L. H.; Voogt, F. C.; Hibma, T.; Sawatzky, G. A. *Phys. Rev. B* **1999**, *59*, R2517.
(12) Altieri, S.; Tjeng, L. H.; Sawatzky, G. A. *Thin Solid Films* **2001**, *400*, 9.
(13) Valeri, S.; Altieri, S.; Di Bona, A.; Giovanardi, C.; Moia, T. S. *Thin Solid Films* **2001**, *400*, 16.
(14) Altieri, S.; Tjeng, L. H.; Voogt, F. C.; Hibma, T.; Rogojanu, O.; Sawatzky, G. A.; *Phys. Rev. B* **2002**, *66*, 155432.
(15) Huang, H. H.; Jiang, X.; Siew, H. L.; Chin, W. S.; Sim, W. S.; Xu, G. Q. *Surf. Sci.* **1999**, *436*, 167.
(16) Malik, I. J.; Hrbek, J.; Shek, M.-L.; Bzowski, A.; Kristof, P.; Sham, T. K. *J. Vac. Sci. Technol., A* **1992**, *10*, 2367.
(17) Ochs, D.; Maus-Friedrichs, W.; Brause, M.; Günster, J.; Kempter, V.; Puchin, V.; Shluger, A.; Kantorovich, L. *Surf. Sci.* **1996**, *365*, 557.
(18) Günster, J.; Stultz, J.; Krischok, S.; Goodman, D. W.; Stracke, P.; Kempter, V. *J. Vac. Sci. Technol., A* **1999**, *17*, 1657.
(19) Robey, S. W. *J. Vac. Sci. Technol., A* **1998**, *16*, 2423.
(20) Yadavalli, S.; Yang, M. H.; Flynn, C. P. *Phys. Rev. B* **1990**, *41*, 7961.
(21) Dohnálek, Z.; Kimmel, G. A.; Joyce, S. A.; Ayotte, P.; Smith, R. S.; Kay, B. D. *J. Phys. Chem. B* **2001**, *105*, 3747.
(22) Dohnálek, Z.; Smith, R. S.; Kay, B. D. *J. Phys. Chem. B* **2002**, *106*, 8360.
(23) Schintke, S.; Messerli, S.; Pivetta, M.; Patthey, F.; Libioulle, L.; Stengel, M.; De Vita, A.; Schneider, W.-D. *Phys. Rev. Lett.* **2001**, *87*, 276801.
(24) Valeri, S.; Altieri, S.; Del Pennino, U.; Di Bona, A.; Luches, P.; Rota, A. *Phys. Rev. B* **2002**, *65*, 245410.
(25) Valeri, S.; Altieri, S.; Di Bona, A.; Luches, P.; Giovanardi, C.; Moia, T. S. *Surf. Sci.* **2002**, *507*−*510*, 311.
(26) Gallagher, M. C.; Fyfield, M. S.; Cowin, J. P.; Joyce, S. A. *Surf. Sci.* **1995**, *339*, L909.
(27) Dohnálek, Z.; Kimmel, G. A.; McCready, D. E.; Young, J. S.; Dohnálková, A.; Smith, R. S.; Kay, B. D. *J. Phys. Chem. B* **2002**, *106*, 3526.
(28) Huang, L.; Chey, S. J.; Weaver, J. H. *Phys. Rev. Lett.* **1998**, *80*, 4095.
(29) Antonov, V. N.; Palmer, J. S.; Bhatti, A. S.; Weaver, J. H. *Phys. Rev. B* **2003**, *68*, 205418.
(30) Yan, X.-M.; Ni, J.; Robbins, M.; Park, H.; Zhao, W.; White, J. M. *J. Nanopart. Res.* **2002**, *4*, 525.
(31) Grunze, M.; Ruppender, H.; Elshazly, O. *J. Vac. Sci. Technol., A* **1988**, *6*, 1266.
(32) Chambers, S. A. *Surf. Sci. Rep*. **2000**, *39*, 105.
(33) King, D. E. *J. Vac. Sci. Technol., A* **1995**, *13*, 1247.
(34) Krozer, A.; Rodahl, M. *J. Vac. Sci. Technol., A* **1997**, *15*, 1704.
(35) Koslowski, B.; Boyen, H.-G.; Wilderotter, C.; Kastle, G.; Ziemann, P.; Wahrenberg, R.; Oelhafen, P. *Surf. Sci.* **2001**, *475*, 1.
(36) *CRC Handbook of Chemistry and Physics*, 73rd ed.; CRC Press: Boca Raton, FL, 1992.
(37) Namba, H.; Darville, J.; Gilles, J. M. *Surf. Sci.* **1981**, *108*, 446.
(38) Zangwill, A. *Physics at Surfaces*; Cambridge University Press: Cambridge, 1988.
(39) Stevenson, K. P.; Kimmel, G. A.; Dohnálek, Z.; Smith, R. S.; Kay, B. D. *Science* **1999**, *283*, 1505.
(40) Kimmel, G. A.; Stevenson, K. P.; Dohnálek, Z.; Smith, R. S.; Kay, B. D. *J. Chem. Phys*. **2001**, *114*, 5284.
(41) Volmer, M.; Weber, A. *Z. Phys. Chem.* **1926**, *119*, 277.
(42) Vidali, G.; Ihm, G.; Kim, H.-Y.; Cole, M. W. *Surf. Sci. Rep.* **1991**, *12*, 133.
(43) Bruch, L. W.; Cole, M. W.; Zaremba, E. *Physical Adsorption: Forces and Phenomena*; Clarendon Press: Oxford, 1997.
(44) Massalski, T. B.; Okamoto, H. *Binary Alloy Phase Diagram*; ASM International: Materials Park, OH, 1990.